THE JOURNAL OF PHYSICAL CHEMISTRY B

Article

pubs.acs.org/JPCB

Simple Liquid Models with Corrected Dielectric Constants

Christopher J. Fennell,* Libo Li, and Ken A. Dill

Laufer Center for Physical and Quantitative Biology, Stony Brook University, Stony Brook, New York 11794, United States

Supporting Information

ABSTRACT: Molecular simulations often use explicit-solvent models. Sometimes explicit-solvent models can give inaccurate values for basic liquid properties, such as the density, heat capacity, and permittivity, as well as inaccurate values for molecular transfer free energies. Such errors have motivated the development of more complex solvents, such as polarizable models. We describe an alternative here. We give new fixed-charge models of solvents for molecular simulations—water, carbon tetrachloride, chloroform, and dichloromethane. Normally, such solvent models are parametrized to agree with experimental values of the neat liquid density and enthalpy of vaporization. Here, in addition to those properties, our parameters are chosen to give the correct dielectric constant. We find that these new parametrizations also happen to give better values for other properties, such as the self-diffusion coefficient. We believe that parametrizing fixed-charge solvent models to fit experimental dielectric constants may provide better and more efficient ways to treat solvents in computer simulations.

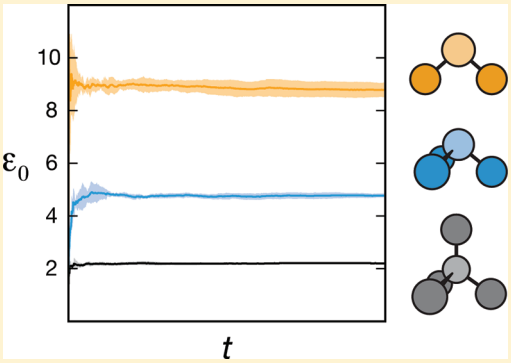

1. INTRODUCTION

In molecular simulations, solvents such as water are often represented by explicit models such as TIP3P or SPC.[1,2] Many of these explicit-solvent models were originally developed and parametrized a few decades ago. They were parametrized to agree with experimental data such as the density and enthalpy of vaporization of the neat liquid, key quantities that are readily available from accurate experiments. However, such molecular solvent models do not typically predict the correct experimental value of the dielectric constant.[3−7] This is unfortunate because molecular simulations are so commonly used to treat the solvation of polar and charged molecules, for which it is essential that the solvent respond properly to electrostatic fields. Reproducing the dielectric constant is especially critical in low-dielectric solvents like chloroform or cyclohexane. While solvents with dielectric constants of 80 and 60 can give solvation free energies of a charge within 1% of one another, solvents with dielectric constants of 2 and 1.5 will give solvation free energies that are more than 50% different.

When current solvent models fail to reproduce the dielectric constant, it is often concluded that improvement can only be achieved by resorting to more complicated geometries or additional interactions, such as those present in expensive polarizable or quantum chemical models[5,6,8−15] We take a different approach here. Here, we develop classical fixed-charge molecular solvent models for water, CCl_4, $CHCl_3$, and CH_2Cl_2, but we parametrize them based on experimental dielectric constants, in addition to the solvent density and enthalpy of vaporization. We find that our newly parametrized solvent models capture some additional experimental properties at least as well as previous models, in addition to getting the dielectric constant correct. The benefit of reparametrized fixed-charge models is that it allows for much more efficient simulations than those involving polarizable or QM force fields.

We develop molecular models of carbon tetrachloride ($\varepsilon(0)$ = 2.2 at 298.15 K and 1 atm), chloroform ($\varepsilon(0)$ = 4.7), dichloromethane ($\varepsilon(0)$ = 8.9), and water ($\varepsilon(0)$ = 78.4). Our choice of which solvents to model was based on wanting a wide range of dielectric constants and wanting no more than two primary atom types. The latter is so that we can test our parametrization methodology for incorporating experimental dielectric constant information without the extra complexity or additional parameters that would be needed for multiatom type solvents.

2. METHODS

2.1. Building Initial Molecular Structures. For the chloromethanes, we start with the gas-phase geometry, and for water, we used both the gas-phase geometry as in TIP3P water[1] and the simplified tetrahedral geometry of SPC water.[2] As chloroform and dichloromethane contain three atom types, we chose to work with united-atom variants to simplify the liquids to two atom types, and compare how well an optimized united-atom model reproduces experimental quantities relative to an existing all-atom model.

To start the model optimization process, we first need an initial set of parameters. These include Lennard-Jones (LJ) σ_{LJ} and ε_{LJ} parameters for each atom type, as well as an initial

Special Issue: Harold A. Scheraga Festschrift

Received: January 8, 2012
Revised: March 1, 2012
Published: March 7, 2012

dx.doi.org/10.1021/jp3002383 | J. Phys. Chem. B 2012, 116, 6936−6944

distribution of partial charges. For each of these, we chose experimentally derived or simple values. As the σ_{LJ} parameter corresponds to an atom size, we chose the Bondi radii as the initial LJ radius, or $\sigma_{LJ}/2$.[16] For united-atom sites in CH_2Cl_2 and $CHCl_3$, we calculated the initial van der Waals volume of the all-atom versions of these molecules using a mutual overlapping spheres procedure.[17] We then placed the united-atom (UA) site at the center of mass of the carbon and hydrogen atoms and scaled the size of this UA site until the new volume of the molecule was equal to the all-atom van der Waals volume (see Figure 1). As these molecules consist of

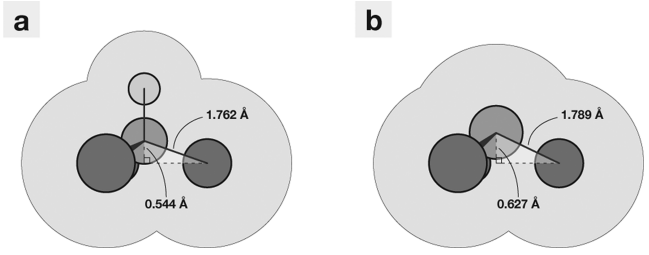

Figure 1. (a) The initial gas-phase geometry representation of chloroform and (b) the resulting united atom representation.

only two atom types, we distributed charges evenly among like atoms in accordance with the experimentally determined gas-phase molecular dipole moments. Finally, there are several avenues that one could take for assigning ε_{LJ} parameters for atom types. The ε_{LJ} parameter corresponds to an atom's dispersion attraction, and one could assign relative depths based on polarizability, electronegativity, or even the number of valence electrons.[18] We have opted for the simpler route of assigning the same ε_{LJ} value to all atom types.

2.2. Optimization Procedure. The typical route for developing molecular models for liquid simulations is to focus on matching the density, enthalpy of vaporization (ΔH_{vap}), and possibly another property like the self-diffusion coefficient or liquid structure.[1−3,6,7,10,19−21] Here we aim for agreement also with the dielectric constant, in addition to the experimental density and ΔH_{vap}. To show how these molecular models can be made to agree with these experimental quantities, we uniformly scaled the σ_{LJ} values, charge magnitudes, and ε_{LJ} values and calculated how the properties changed. An example illustrating how scaling of these parameters affects these properties is shown in Figure 2. Starting from the constructed united-atom CH_2Cl_2 model, it is apparent that both the density (ρ) and dielectric constant ($\varepsilon(0)$) are sharply dependent upon the size of the molecule. However, when the charge magnitudes (q) are uniformly scaled, the dielectric constant is affected to a much greater degree than the density. Finally, ε_{LJ} changes primarily affect ΔH_{vap} mostly independent of the other properties. This gives a prescription for sequential optimization of the model parameters for fitting to the experimental properties of interest.

(1) Fit ρ by uniformly scaling all the σ_{LJ} values.
(2) Fit $\varepsilon(0)$ by uniformly scaling all the q values.
(3) Fit ΔH_{vap} by uniformly scaling all the ε_{LJ} values.

Each step of this optimization process involves a linear fitting procedure in the specific parameter space of interest. For example, the initial process of fitting the density involves an initial simulation with the starting set of parameters and a check to see if it is greater or less than the target value. If the liquid is too dense, the σ_{LJ} values are all increased by 5% to expand the system, and the density is recomputed after another simulation. We then linearly interpolate to find the σ_{LJ} scaling that corresponds to the target density. Since the relations between properties and parameters are not strictly linear, multiple interpolation steps using the current and previous step information are often needed to fit a given parameter. Typically, we see convergence on a given property to a specified tolerance within two to four interpolation steps.

It is apparent in Figure 2 that the liquid properties are not exclusively dependent upon single model parameters—changing one of the parameters will have some effect on all of the properties. This means that this sequence needs to be iterated to focus in on the optimal set of experimental properties. The amount of iteration depends on the degree to which the parameters are correlated with the properties and the width of the specified tolerances. Table 1 lists the target properties for all the liquids and fitting tolerance for each. For the chloromethanes, convergence was typically achieved within two or three iterations. Water properties tended to be more

Table 1. Experimental Properties at 298 K and 1 atm[22] and Fitting Tolerances for the Investigated Liquids

	ρ tolerance (kg/m^3)		ΔH_{vap} tolerance (kJ/mol)		$\varepsilon(0)$	tolerance
CCl_4	1587	±2	32.45	±0.5	2.23	±0.15
$CHCl_3$	1473	±2	31.30	±0.5	4.71	±0.15
CH_2Cl_2	1317	±2	28.82	±0.5	8.93	±0.15
H_2O	997	±2	43.99	±0.5	78.4	±1.5

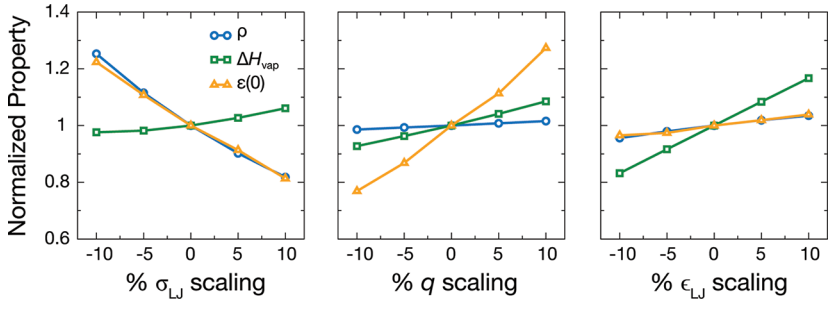

Figure 2. The variation of the normalized density (ρ), enthalpy of vaporization (ΔH_{vap}), and dielectric constant ($\varepsilon(0)$) of CH_2Cl_2 as a function of uniform parameter variation. As the LJ σ_{LJ} (left) is scaled, both ρ and $\varepsilon(0)$ sharply vary. When the charge magnitude (middle) and LJ ε_{LJ} (right) are scaled, only $\varepsilon(0)$ and ΔH_{vap} sharply vary, respectively.

dx.doi.org/10.1021/jp3002383 | J. Phys. Chem. B 2012, 116, 6936−6944

correlated to the model parameters, so five or more iterations were not uncommon.

Solutions found by this optimization procedure are not necessarily unique, particularly given that there is an allowed tolerance window for each property. Despite this, multiple optimizations involving different initial dipole moments all ended with similar final parameters.

2.3. CCl_4 Poses a Challenge. CCl_4 poses an interesting challenge for our present approach. CCl_4 is tetrahedral and symmetric. It has no dipole moment in the gas phase. Without a dipole moment, a rigid fixed-charge liquid model will have a dielectric constant $\varepsilon(0)$ close to 1. However, CCl_4 has a dielectric response ($\varepsilon(0) > 2$). It and other nonpolar liquids have apparent dipolar character in the liquid state.[23] This situation has motivated the recent development of polarizable models for CCl_4 and for other low-dielectric liquids.[14,15] In order to retain the advantages of fixed-charge force fields, our approach here instead is to include a permanent dipole in the model. Such a dipole moment will likely be different than an experimentally measured dipole moment for CCl_4, as it will incorporate the polarizable contributions to the permittivity.

There are different ways to incorporate a dipole in CCl_4. We explored all the possibilities for distributing the positive and negative partial charges of a dipole throughout the atoms in a molecule having this symmetry. All models successfully fit the experimental data and exhibited identical experimental properties that were not part of the fitting procedure. In the interest of simplicity, we only discuss two of the models, illustrated in Figure 3. In these models, the dipole is either localized along one of the C−Cl bonds or distributed across three of them. All plotted data below is from the simpler localized model (Figure 3a).

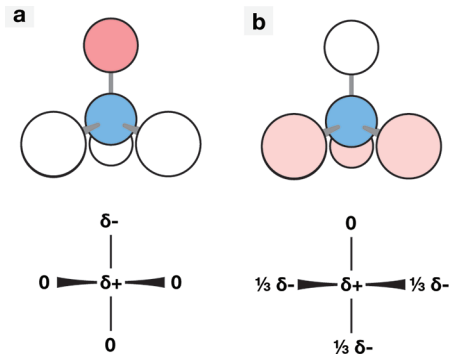

Figure 3. The (a) localized and (b) distributed dipole models for CCl_4. The localized model places the positive charge on the carbon atom and the negative on a single chlorine, while the distributed model splits the negative charge over three of the chlorine atoms.

2.4. Simulation Details. All molecular dynamics calculations were performed using version 4.5.5 of the GROMACS molecular dynamics package.[24,25] The leapfrog algorithm with time steps of 4 fs for chloromethane and 2 fs for water simulations was used to integrate the equations of motion. The chloromethane models were held rigid using the SHAKE algorithm,[26] while the water models were held rigid using the SETTLE algorithm.[27] The isothermal−isobaric ensemble (*NPT*) using the Nose−Hoover thermostat and the Parrinello−Rahman barostat was used in both the optimization and temperature dependent property simulations. Dynamical properties were also computed from these simulations, and these properties were independently verified with sets of microcanonical (*NVE*) ensemble simulations. Long-range electrostatics were handled using the smooth version of the particle mesh Ewald (PME) method[28] under tinfoil boundary conditions with a grid spacing of 0.12, a PME order of 4, an Ewald parameter energy tolerance of 10^{-5}, and a real-space cutoff of 15 Å for chloromethane and 12 Å for water simulations. The Lennard-Jones (LJ) interactions were switched off from 10 to 12 Å for the chloromethane and 8 to 10 Å for water simulations, and energy and pressure tail corrections were included in all cases. As seen by others,[29,30] the longer LJ cutoff is necessary to achieve converged system densities. Lorentz−Berthelot mixing rules were used to compute mixed-LJ interactions between differing atom types.

Optimization simulations involved rhombic dodecahedral boxes of 325 molecules for chloromethane simulations and cubic boxes of 650 molecules for water simulations. All of these simulations were carried out at 298.15 K and 1 atm. Run-time lengths ranged from 1 ns for density and ΔH_{vap} optimization to 10 ns for $\varepsilon(0)$ optimization. System size effects were investigated with the final parameter sets by calculating properties for systems with 4 times the number of atoms with increasingly larger interaction cutoff radii, and property results were identical within error to those from these smaller systems. The calculated final properties are averages from five independent 10 ns simulations, and standard errors are reported for these averages. For the water models, we also extended the 298.15 K simulations out to 50 ns to test the convergence of $\varepsilon(0)$. All calculated properties for water at 298.15 K come from these longer simulations.

2.5. Calculation of Liquid Properties. With proper sampling of the given ensemble, thermodynamic and dynamic properties can be computed from fluctuations over the course of the simulation. In addition to the density, the following properties were calculated for all the optimized models.

2.5.1. Enthalpy of Vaporization. The enthalpy of vaporization is traditionally computed from the difference between the enthalpy of an ideal gas and the liquid state

$$\Delta H_{vap}(T) = H(T)_{ideal} - H(T)_{liq} = -\langle E_{liq}\rangle/N + RT \quad (1)$$

where E_{liq} is the total intermolecular energy of the system of N molecules, R is the ideal gas constant, and T is the temperature. Others have noted that more detailed estimations of ΔH_{vap} can be determined by including nonclassical and nonideal gas corrections.[6] We decided to use the traditional approximation as it corresponds to the heat required to vaporize these nonpolarizable models in simulations, though including such corrections could lead to improved agreement with experimental properties.

2.5.2. Static Dielectric Constant. For nonpolarizable liquids, $\varepsilon(0)$ can be calculated from fluctuations of the total system dipole moment ($\mathbf{M}$) according to

$$\varepsilon(0) = 1 + \frac{4\pi}{3k_B T\langle V\rangle}(\langle \mathbf{M}^2\rangle - \langle \mathbf{M}\rangle^2) \quad (2)$$

where k_B is the Boltzmann constant and V is the total system volume.[31] One difficulty in calculating $\varepsilon(0)$ is that it is accumulated as a running average and will typically not converge over subnanosecond simulations. We needed to perform 10 ns simulations in order to obtain consistent estimates of $\varepsilon(0)$ for all liquids.

dx.doi.org/10.1021/jp3002383 | J. Phys. Chem. B 2012, 116, 6936−6944

Table 2. Model Parameters for CCl_4-DC with a Localized Dipole (L), CCl_4-DC with a Distributed Dipole (D), $CHCl_3$-DC, and CH_2Cl_2-DC

model	atom type	constraint	d (Å)	q (e^-)	σ (Å)	ε (kJ/mol)
CCl_4-DC (L)	C			0.14780	4.06640	0.587072
	CL			−0.14780 and 0	4.18602	0.587072
		C-CL	1.7670			
		CL-CL	2.8855			
CCl_4-DC (D)	C			0.22542	4.06830	0.585791
	CL			−0.07514 and 0	4.18796	0.585791
		C-CL	1.7670			
		CL-CL	2.8855			
$CHCl_3$-DC	UA			0.55179	3.73400	1.078200
	CL			−0.18393	3.58871	1.078200
		UA-CL	1.7894			
		CL-CL	2.9028			
CH_2Cl_2-DC	UA			0.40440	3.71813	1.281890
	CL			−0.20220	3.53079	1.281890
		UA-CL	1.8215			
		CL-CL	2.9344			

Table 3. Liquid Properties for Chloromethanes Calculated at 298.15 K and 1 atm with the Standard Error of the Last Digit in Parentheses

liquid	model	ρ (kg/m^3)	ΔH_{vap} (kJ/mol)	$\varepsilon(0)$	C_p (J/mol·K)	κ_T (10^6 atm^{-1})	α_p (10^5 K^{-1})	D (10^{-9} m^2/s)	μ (D)
CCl_4	CCl_4-DC (L)	1588.7 (1)	32.392 (3)	2.202 (6)	154 (2)	134 (2)	213 (4)	1.24 (2)	1.26
	CCl_4-DC (D)	1588.77 (7)	32.406 (1)	2.112 (8)	156 (2)	137 (2)	219 (4)	1.26 (3)	1.23
	Fox	1626.6 (5)	34.51 (1)	1.0302 (2)	120 (1)	102 (3)	126 (3)	1.73 (3)	0.23
	expt	1587[a]	32.43[a]	2.228[a]	130.7[a]	111[b]	116[b]	1.4[c]	
$CHCl_3$	$CHCl_3$-DC	1471.16 (7)	31.222 (4)	4.77 (3)	85 (1)	78 (2)	116 (2)	1.48 (3)	1.66
	Fox	1476.7 (2)	30.119 (6)	4.39 (1)	118 (1)	121 (4)	244 (5)	2.74 (8)	1.40
	expt	1473[a]	31.28[a]	4.711[a]	114.2[a]	106[b]	123[b]	2.3,[d] 2.5[e]	
CH_2Cl_2	CH_2Cl_2-DC	1316.34 (1)	28.740 (1)	8.8 (1)	92.3 (8)	98 (1)	159 (2)	2.13 (2)	2.10
	Fox	1265.9 (4)	25.95 (1)	8.65 (3)	118 (1)	158 (1)	180 (2)	4.11 (5)	2.01
	expt	1317[a]	28.82[a]	8.93[a]	101.2[a]	104[a]	139[a]	3.3 (2)[f]	

[a]Reference 22. [b]Interpolated to 298.15 K from data in ref 22. [c]Reference 34. [d]Reference 35. [e]Reference 36. [f]Reference 37.

2.5.3. C_p, κ_T, and α_p. As an additional test of thermodynamic quantities for the resulting models, we computed the isobaric heat capacity (C_p), the isothermal compressibility (κ_T), and the thermal expansion coefficient (α_p). These were calculated using the following fluctuation formulas from *NPT* simulations

$$C_p = \left(\frac{\partial H}{\partial T}\right)_{N,P} = \frac{\langle H^2\rangle - \langle H\rangle^2}{Nk_BT^2} + 3R \tag{3}$$

$$\kappa_T = -\frac{1}{V}\left(\frac{\partial V}{\partial P}\right)_{N,T} = \frac{\langle V^2\rangle - \langle V\rangle^2}{k_BT\langle V\rangle} \tag{4}$$

$$\alpha_p = \frac{1}{V}\left(\frac{\partial V}{\partial T}\right)_{N,P} = \frac{\langle VH\rangle - \langle V\rangle\langle H\rangle}{k_BT^2\langle V\rangle} \tag{5}$$

2.5.4. Self-Diffusion Coefficient. The self-diffusion coefficient was calculated for all the models alongside the above thermodynamic quantities. D was calculated from a regression fit to the linear region (0.5−6 ns) of a plot of the Einstein relation[32]

$$D = \lim_{t\to\infty} \frac{\langle|\mathbf{r}_i(t) - \mathbf{r}_i(0)|^2\rangle}{6t} \tag{6}$$

where $\mathbf{r}_i(t)$ is the position of the center of mass of molecule i at time t. Dynamical quantities are typically calculated from *NVE* simulations in order to avoid perturbations introduced by thermostats and barostats. We calculated D for all models from *NVE* simulations near 298.15 K and 1 atm, and found that they were identical to the *NPT* simulations used for the above thermodynamic quantities. This indicated that the thermostat and barostat coupling was weak enough to not significantly perturb the dynamics. We report D results from the *NPT* simulations for simplicity.

2.5.5. Structural Analysis. Finally, we calculated radial distribution functions between various atom types for comparisons with other models and experimental scattering data. These distribution functions were calculated by binning separation distances (r_{ij}) between atoms of type A and B via

$$g_{AB}(r) = \frac{1}{N_A\langle\rho_B\rangle}\sum_{i\in A}^{N_A}\sum_{j\in B}^{N_B}\frac{\delta(r_{ij} - r)}{4\pi r^2} \tag{7}$$

where ρ_B is the bulk system density of atom type B.

3. RESULTS AND DISCUSSION

Table 2 gives the values of our parameters for the nonpolar solvents we modeled, and Table 3 compares the properties we calculate from our models compared to all-atom RESP models from Fox and Kollman[30] and to experiments. The models from the present work are labeled with DC to indicate that they are "dielectric corrected". The Fox models are flexible all-atom

dx.doi.org/10.1021/jp3002383 | J. Phys. Chem. B 2012, 116, 6936−6944

models—they allow harmonic bond stretching and angle bending motions—that are derived from the AMBER force field.[33] The values reported here differ considerably from those published (specifically the self-diffusion constant). This difference comes from the expanded sampling in these simulations that provides a better estimate of the actual thermodynamic and dynamic properties of the models.

All the DC models shown in Table 3 are converged on the experimental density, ΔH_{vap}, and dielectric constant to within the previously stated tolerances. The dielectric constant was the slow step in the fitting process. Figure 4 shows the running

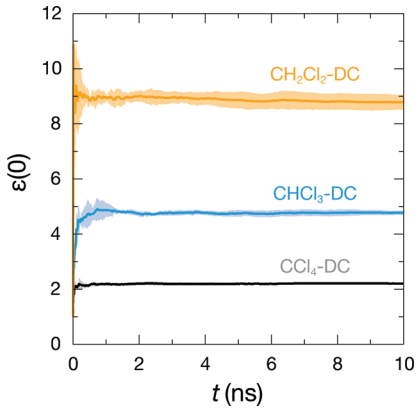

Figure 4. The static dielectric constant for the DC chloromethane models over the course of 10 ns of molecular dynamics at 298.15 K and 1 atm. The lines are averages of five simulations, and the shaded regions show the standard deviation of these averages.

average of the $\varepsilon(0)$ values, over the course of 10 ns of molecular dynamics. The lines are average traces over five simulations, and the shaded region shows the standard deviation of these averages. While the dielectric constant of CCl_4 levels quickly and the deviations are barely visible, the CH_2Cl_2 trace shows the difficulty in fitting when considering liquids with higher dielectric constants. At the end of the 10 ns, the standard deviation is still roughly ±0.2 dielectric units, very close to the size of our tolerance window for convergence. To fit the dielectric to a tighter window, we would need proportionally longer simulation times. If we wanted to work with a material with a larger dielectric constant, we would either need a looser $\varepsilon(0)$ convergence criterion or longer simulation lengths.

3.1. Adding a Dipole Improves the Permittivity of CCl_4. In Table 3, there is a noticeable trend of increasing dipole moment with increasing $\varepsilon(0)$ from CCl_4 down to CH_2Cl_2. This trend has been recognized in the past,[5,21,38] and it simply follows that the greater the partial charges, the greater the screening ability of the liquid. This result holds true for the flexible all-atom models as well, as they have lower average dipole moments than the analogous DC models and consistently under-predict the dielectric constant. In the case of CCl_4, the embedded dipole actually allows the DC models to express $\varepsilon(0)$ in line with experiment. Both the thermodynamic and dynamic properties are nearly identical for the localized and distributed CCl_4 models, as are the dipole moments for the two models. These results indicate that the geometry of the charge distribution that makes the dipole moment is less important than the magnitude.

As the CCl_4-DC models are fit to experimental density, ΔH_{vap}, and $\varepsilon(0)$ quantities, it is not surprising that they reproduce these quantities better than the all-atom model. The Fox and Kollman model captured a small fraction of the permittivity, as it is flexible and has a small dipole moment in the liquid phase. While the diffusivity relative to experiment for CCl_4-DC is improved over the flexible model, α_p for the CCl_4-DC models is considerably degraded. Embedding a dipole had the effect of increasing the σ_{LJ} values on the atoms, and this makes the volume of the liquid more sensitive to temperature changes. This results in the liquid having a less tightly structured first solvation shell than the flexible Fox and Kollman model (see the Supporting Information) and a possibly less accurate fit to neutron scattering experiments.[39]

3.2. United-Atom Chloromethanes Behave Similarly to All-Atom Models. In addition to corrected dielectric versions of these liquids, we were interested in united-atom variants of $CHCl_3$ and CH_2Cl_2 that could work as a more efficient mimic of a detailed all-atom model. The results in Table 3 indicate this to be the case. Not surprisingly, the DC models fit well the experimental data to which they were matched. More interesting, however, is the observation that these new models do well at reproducing other thermodynamic properties of the real liquid that were not part of the parametrization exercise, often better than the more detailed Fox and Kollman models. While structural comparisons between united-atom and all-atom models are inexact, a qualitative radial distribution function comparison indicates that both $CHCl_3$-DC and CH_2Cl_2-DC are more structured than the flexible all-atom Fox and Kollman models (see the Supporting Information). This is likely due to the enhanced dipole moments of the dielectric corrected models, resulting in stronger pair interactions and larger ΔH_{vap} values. These results indicate that, even with a less complex model geometry, correcting for the dielectric has additional advantages.

3.3. The DC Chloromethane Models Capture Some of the Temperature Dependence of $\varepsilon(0)$. These DC models, like other liquid models, are fit to one temperature. We tested how well our DC models capture the temperature dependence of the dielectric constant, in 5 K increments within the available range of experimental data for $\varepsilon(0)$; see Figure 5. At a fitting

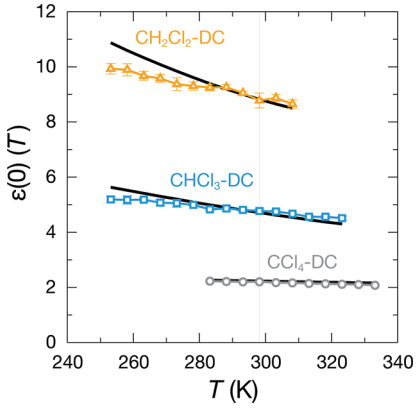

Figure 5. The temperature dependence of $\varepsilon(0)$ for the DC chloromethane models compared with experimental data.[22] The black lines are the experimental curves for each liquid shown.

temperature of 298.15 K, all the models match with experiments. All the models have the correct sign of the slope: $\varepsilon(0)$ decreases with increasing temperature. At low temperatures, the CH_2Cl_2 and $CHCl_3$ models deviate from the

dx.doi.org/10.1021/jp3002383 | J. Phys. Chem. B 2012, 116, 6936−6944

Table 4. Model Parameters for SPC/DC and H_2O-DC

model	atom type	constraint	d (Å)	q (e^-)	σ (Å)	ε (kJ/mol)
SPC/DC	O			−0.87362	3.15767	0.822882
	H			0.43681	0.00000	0.000000
		O−H	1.00000			
		H−H	1.63299			
H_2O-DC	O			−0.90990	3.18400	0.593000
	H			0.45495	0.00000	0.000000
		O−H	0.95800			
		H−H	1.56441			

Table 5. Liquid Properties for Water Calculated at 298.15 K and 1 atm with the Standard Error of the Last Digit in Parentheses

model	ρ (kg/m^3)	ΔH_{vap} (kJ/mol)	$\varepsilon(0)$	C_p (J/mol·K)	κ_T (10^6 atm^{-1})	α_p (10^5 K^{-1})	D (10^{-9} m^2/s)	μ (D)
SPC	978.41 (3)	36.820 (1)	65.6 (2)	82.9 (3)	53.7 (5)	71.5 (7)	3.99 (1)	2.27
SPC/E	999.53 (2)	41.905 (1)	71.1 (1)	86.3 (2)	46.1 (2)	49.1 (4)	2.46 (1)	2.35
SPC/DC	998.69 (2)	43.993 (1)	78.3 (6)	83.2 (3)	43.7 (3)	48.8 (9)	2.48 (1)	2.42
H_2O−DC	997.55 (2)	43.366 (1)	78.7 (6)	87.8 (2)	45.0 (2)	44.8 (4)	2.17 (1)	2.42
Expt	997.5[a]	43.99[a]	78.36[a]	75.3[a]	45.84[a]	25.6[a]	2.299[b]	

[a]Reference 22. [b]Reference 43.

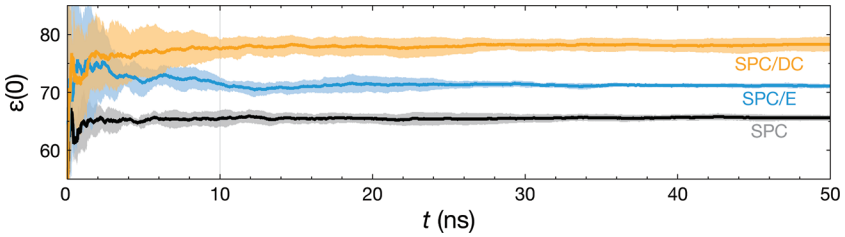

Figure 6. The static dielectric constant for SPC (black line), SPC/E (blue line), and SPC/DC (gold line) over the course of 50 ns of molecular dynamics at 298.15 K and 1 atm. The lines are averages of five simulations, and the shaded regions show the standard deviation of these averages. The plots show that the models have difficulty converging $\varepsilon(0)$ on time-scales less than 10 ns, the length of simulations in our dielectric correction procedure. Longer simulations would likely aid in optimization processes set to converge on a high $\varepsilon(0)$.

experimental $\varepsilon(0)$ values, while the CCl_4-DC model results (localized dipole model shown in Figure 5) are quantitative across the entire available range.

3.4. Applying the Dielectric Correction to Water Models. We were interested to see if we could improve upon current water models, by correcting their dielectric constants in the manner described above. We considered two water models: TIP3P ($\varepsilon(0) > 90$) and SPC ($\varepsilon(0) < 70$).[40]

The atom sites in TIP3P are arranged in the experimental gas-phase geometry, and from a property standpoint, the density is less than experiment and $\varepsilon(0)$ is greater than experiment. We would therefore expect both the σ parameter and charge magnitudes to decrease in order to align with experiment. Indeed, these changes occur; however, the intermediate models rapidly crystallize into face-centered cubic lattices. We tested multiple starting states (larger and smaller σ and q values), and this crystallization was repeatable in all cases. Weakening the electrostatic interaction in TIP3P to match the experimental $\varepsilon(0)$ eliminates its ability to effectively hydrogen-bond. This observation appears to agree with findings showing alteration of the bond angle of SPC/E below 105° (the bond angle of TIP3P is 104.5) and above 115° causes a breakdown in the liquid properties.[41,42] This also corresponds to how other researchers have been successful in modifying the TIP4P model to better reproduce liquid and phase behavior properties.[6,7] By having the negative partial charge offset from the Lennard-Jones site center, TIP4P models are effectively more tetrahedral than the gas-phase geometry suggests.

The atom sites in SPC are perfectly tetrahedral, and the dielectric correction procedure was able to converge on a liquid-state model. The resulting parameters for SPC/DC are listed in Table 4. In addition to this SPC geometry based model, we show the resulting parameters for a tetrahedral model that has O−H bond lengths equal to the experimental gas-phase value (also the TIP3P value). We refer to this model as H_2O-DC, and it is a hybrid water model that probes both how SPC would respond to having bond lengths in better agreement with experiment and how TIP3P would respond with a more tetrahedral geometry. Properties at 298.15 K and 1 atm are listed in Table 5 alongside those for SPC, SPC/E, and experiment.

3.5. Optimized SPC Resembles Models with Lower Dielectric Constants. When the SPC/E water model was originally developed, the authors recognized the need for an added extended polarization interaction to the SPC model.[19] They incorporated this effect by uniformly increasing the charge magnitude on the atom sites, keeping all other model parameters the same. This changed the dipole moment from 2.27 to 2.35 D and subsequently improved most of the structural, thermodynamic, and dynamic properties. This increase in the dipole moment is the maximum possible without increasing the density of the liquid above 1 g/cm^3. One point of note shown in Table 5 is the increase in $\varepsilon(0)$ from 66 to 71. To bring the SPC model $\varepsilon(0)$ up to the experimental value, the charge magnitudes need to be scaled up further, and the other model parameters (namely, σ and ε) will need to be

dx.doi.org/10.1021/jp3002383 | J. Phys. Chem. B 2012, 116, 6936−6944

simultaneously adjusted to compensate for the increasing density. The resulting SPC/DC model parameters shown in Table 4 do exactly this. The oxygen site charge increases from 0.82 to 0.8476 to 0.87362 for SPC, SPC/E, and SPC/DC, respectively, and the LJ parameters are modified to accommodate this additional charge. Figure 6 shows the convergence of $\varepsilon(0)$ over the course of 50 ns of molecular dynamics. These traces further emphasize the difficulty in converging on a specific $\varepsilon(0)$ when working with high dielectric liquids. The standard deviation spread for SPC/DC has reached the ±1.5 dielectric unit tolerance by 10 ns, though the dielectric optimization process would likely be more efficient using longer simulations for more accurate intermediate assessments of $\varepsilon(0)$.

Table 5 shows that our dielectric correction leads to minor improvements of agreement with experiments for most of the thermodynamic and dynamic quantities, compared to SPC/E. Figure 7 shows that the $g_{OO}(r)$, $g_{OH}(r)$, and $g_{HH}(r)$ for these

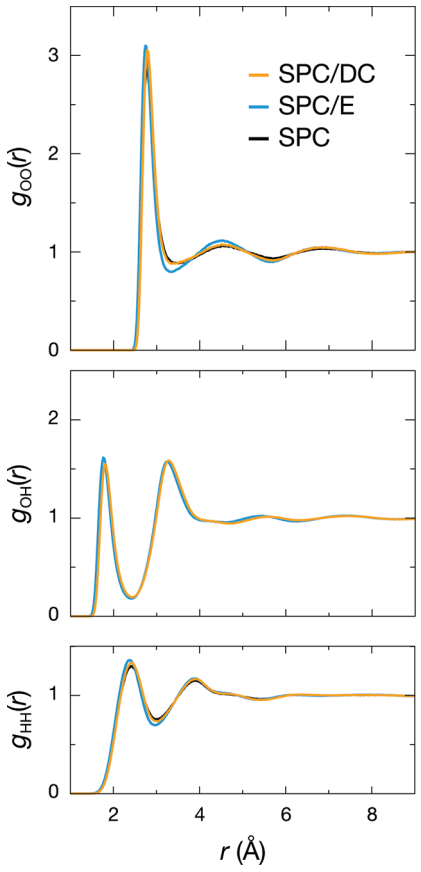

Figure 7. The oxygen−oxygen (top), oxygen−hydrogen (middle), and hydrogen−hydrogen (bottom) radial distribution functions for SPC, SPC/E, and SPC/DC. The SPC and SPC/DC curves overlap tightly in all the plots with the only deviations being slightly enhanced peaking in the $g_{OO}(r)$ and $g_{HH}(r)$.

three water models are nearly superimposable. The SPC and SPC/DC $g(r)$ curves fall right on top of one another in all three plots, while the SPC/E curves are more peaked and have a slightly more ordered second shell. This is likely a degradation in the overall liquid structure as the SPC/E model has been shown to be a better fit to neutron and X-ray scattering data.[44−46]

One possible consideration in matching experimental structural data is the geometry of the particular model. For the SPC models, the OH bond length was simplified to 1 Å, while experimental structural data recommends a value closer to 0.958 Å.[47] Taking this geometry consideration into account, we developed and optimized a tetrahedral model with these OH bond lengths that we call H_2O-DC. While this model has a less converged ΔH_{vap} than SPC/DC, it shows further improvements in most of the other liquid properties. By using shorter OH bond-lengths, we expect and observe some changes in the liquid structure. Figure 8 shows the same

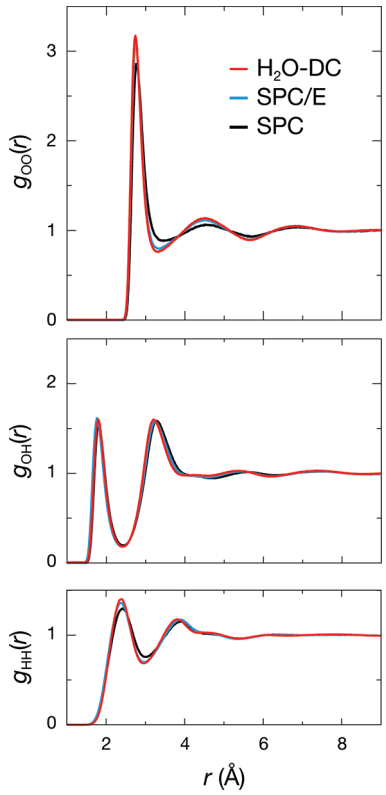

Figure 8. The oxygen−oxygen (top), oxygen−hydrogen (middle), and hydrogen−hydrogen (bottom) radial distribution functions for SPC, SPC/E, and H_2O-DC. The H_2O-DC model is even more structured than SPC/E, making it a potentially better fit to experimental scattering data.

sequence of radial distribution functions as Figure 7, only with H_2O-DC in place of SPC/DC. H_2O-DC is slightly more structured beyond the first solvation shell than SPC/E in all of the curves. This structuring is more in line with scattering data,[44−46,48] making it a potentially truer representation of the real liquid. It should be noted that the first solvation shell for SPC/E type models is typically more peaked than the curves derived from model fits to this experimental scattering data, and this could likely be optimized by using a softer function for the van der Waals potential and/or decreasing the strength of the direct pair-interaction energy.

3.6. DC Water Models Reproduce Temperature Dependent Properties. We looked at the maximum in density as a function of temperature, T_{max}, for these water models. This is experimentally observed at 277 K. Additional interaction sites have been added to some water models to capture this behavior.[6,10] SPC/E also has a T_{max}, though it is

dx.doi.org/10.1021/jp3002383 | J. Phys. Chem. B 2012, 116, 6936−6944

located around 235 K, well below the experimental melting point.[49]

Figure 9 compares the predicted density-maximum temperatures from various models, spanning the supercooled-liquid

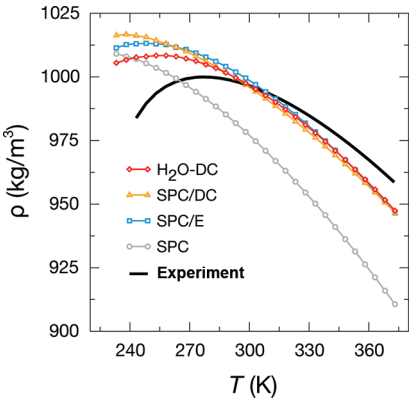

Figure 9. The density of the studied water models as a function of temperature. These fully tetrahedral water models all exhibit a density maximum at a lower temperature than real water,[50,51] though geometric differences between the models indicate a route to correct this flaw.

and liquid phases. Here, the T_{max} for SPC/E is at 247 K. Our computation of this differs from past estimates, likely because the uses of the Ewald summation and LJ pressure correction were not as common when the original estimates were made.[49] As noted in past studies,[52] the SPC model does not exhibit a T_{max} in the temperature range shown, and interestingly, SPC/DC shows a density maximum (calculated from the sign crossover in α_p seen in the Supporting Information) at 239 K, near the edge of the simulated temperature range. Thus, by adopting a liquid structure similar to SPC, this model shows a degradation in the T_{max} relative to SPC/E. The more structured H_2O-DC has a T_{max} at 255 K, closer to experiment than SPC/E. This result indicates that it may be possible to optimize a rigid, three-site water model through geometry distortions and interaction energy scaling to simultaneously reproduce both the $\varepsilon(0)$ and T_{max}.

Figure 10 shows the temperature dependence of $\varepsilon(0)$. The DC models reproduce the experimental $\varepsilon(0)$ at the optimization temperature and the correct trend of decreasing

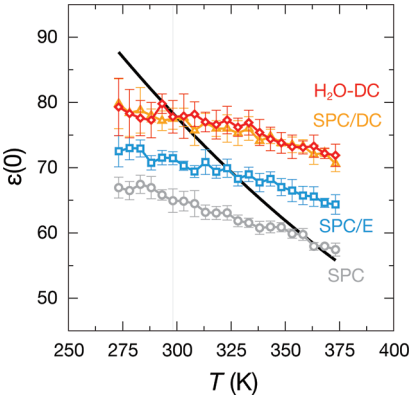

Figure 10. $\varepsilon(0)$ as a function of temperature for the labeled water models alongside experiment[22] (black line). All models capture the trend of decreasing $\varepsilon(0)$ with increasing temperature, though they all fail to reproduce the experimental slope of this trend.

$\varepsilon(0)$ with increasing temperature but not the slope quantitatively. All these models have the same slope, so correcting the dielectric constant at one temperature simply results in a vertical shift of the trend. More complex water models with different interaction site geometries have been shown to better capture the experimental slope,[6,21] so it may be useful in the future to couple changing molecular geometries with the present approach for correcting the dielectrics.

4. CONCLUSIONS

We have developed here parameters for the solvents carbon tetrachloride, a united-atom chloroform, a united-atom dichloromethane, and water for molecular simulations in fixed-charge force fields. The usual approach to development is to choose parameters that cause the molecular simulations of the pure solvent to agree with experiments on the solvent density and enthalpy of vaporization. What is novel here is that our parameters are chosen so that the simulations also give the correct experimental dielectric constants. We find that our models also generally give better agreement with other properties, such as the self-diffusion constant. For water, there is some subtlety. When TIP3P is made to have the correct dielectric constant, it loses the appropriate level of water−water hydrogen bonding. However, when SPC is made to have the correct dielectric constant, it also has improved thermodynamic and dynamic properties. The present work indicates that this approach to parametrizing fixed-charge solvent models for molecular simulations can improve the properties of those solvents relative to older parametrizations. This approach may circumvent the need, at least in some cases, to resort to more expensive polarizable or quantum mechanical solvent models.

■ ASSOCIATED CONTENT

Supporting Information

Model structural comparisons and full tables of temperature dependent property data. This material is available free of charge via the Internet at http://pubs.acs.org.

■ AUTHOR INFORMATION

Corresponding Author

*E-mail: cfennell@gmail.com.

Notes

The authors declare no competing financial interest.

■ ACKNOWLEDGMENTS

We dedicate this paper to Harold Scheraga, who has been such an extraordinary pioneer, gentleman, and mentor to us and so many others. The authors gratefully acknowledge financial support provided by NIH grant GM63592.

■ REFERENCES

(1) Jorgensen, W. L.; Chandrasekhar, J.; Madura, J. D.; Impey, R. W.; Klein, M. L. *J. Chem. Phys.* **1983**, *79*, 926−935.
(2) Berendsen, H. J. C.; Postma, J. P. M.; van Gunsteren, W. F.; Hermans, J. Simple Point Charge Water. In *Intermolecular Forces*; Pullman, B., Ed.; Reidel: Dordrecht, The Netherlands, 1981.
(3) van der Spoel, D.; van Maaren, P. J.; Berendsen, H. J. C. *J. Chem. Phys.* **1998**, *108*, 10220−10230.
(4) Jorgensen, W. L.; Jenson, C. *J. Comput. Chem.* **1998**, *19*, 1179−1186.
(5) Guillot, B. *J. Mol. Liq.* **2002**, *101*, 219−260.

(6) Horn, H. W.; Swope, W. C.; Pitera, J. W.; Madura, J. D.; Dick, T. J.; Hura, G. L.; Head-Gordon, T. *J. Chem. Phys.* **2004**, *120*, 9665−9678.
(7) Abascala, J. L. F.; Vega, C. *J. Chem. Phys.* **2005**, *123*, 234505.
(8) Rick, S. W.; Stuart, S. A.; Bader, J. S.; Berne, B. *J. Mol. Liq.* **1994**, *65/66*, 31−40.
(9) Tironi, G.; Brunne, R. M.; van Gunsteren, W. F. *Chem. Phys. Lett.* **1996**, *250*, 19−24.
(10) Mahoney, M. W.; Jorgensen, W. L. *J. Chem. Phys.* **2000**, *112*, 8910−8922.
(11) Glättli, A.; Daura, X.; van Gunsteren, W. F. *J. Chem. Phys.* **2002**, *116*, 9811−9828.
(12) Glättli, A.; Daura, X.; van Gunsteren, W. F. *J. Comput. Chem.* **2003**, *24*, 1087−1096.
(13) Wu, Y.; Tepper, H. L.; Voth, G. A. *J. Chem. Phys.* **2006**, *124*, 024503.
(14) Lamoureux, G.; Faraldo-Gómez, J. D.; Krupin, S.; Noskov, S. Y. *Chem. Phys. Lett.* **2009**, *468*, 270−274.
(15) Kunz, A.-P. E.; Eichenberger, A. P.; van Gunsteren, W. F. *Mol. Phys.* **2011**, *109*, 365−372.
(16) Bondi, A. *J. Phys. Chem.* **1964**, *68*, 441−451.
(17) Gibson, K. D.; Scheraga, H. A. *J. Phys. Chem.* **1987**, *91*, 4121−4122.
(18) Nagle, J. *J. Am. Chem. Soc.* **1990**, *112*, 4741−4747.
(19) Berendsen, H. J. C.; Grigera, J. R.; Straatsma, T. P. *J. Phys. Chem.* **1987**, *91*, 6269−6271.
(20) Liu, H.; Müller-Plathe, F.; van Gunsteren, W. F. *J. Am. Chem. Soc.* **1996**, *117*, 4363−4366.
(21) Rick, S. W. *J. Chem. Phys.* **2004**, *120*, 6085−6093.
(22) Lide, D. R., Ed. *CRC Handbook of Chemistry and Physics*, 84th ed.; CRC Press, Inc.: Boca Raton, FL, 2004.
(23) Garg, S. K.; Bertie, J. E.; Kilp, H.; Smyth, C. P. *J. Chem. Phys.* **1968**, *49*, 2551−2562.
(24) Berendsen, H. J. C.; van der Spoel, D.; van Drunen, R. *Comput. Phys. Commun.* **1995**, *91*, 43−56.
(25) Hess, B.; Kutzner, C.; van der Spoel, D.; Lindahl, E. *J. Chem. Theory Comput.* **2008**, *4*, 435−447.
(26) Ryckaert, J.; Ciccotti, G.; Berendsen, H. J. C. *J. Comput. Phys.* **1977**, *23*, 327−341.
(27) Miyamoto, S.; Kollman, P. A. *J. Comput. Chem.* **1992**, *13*, 952−962.
(28) Essman, U.; Perela, L.; Berkowitz, M. L.; Darden, T.; Lee, H.; Pedersen, L. G. *J. Chem. Phys.* **1995**, *103*, 8577−8592.
(29) Tironi, I. G.; van Gunsteren, W. F. *Mol. Phys.* **1994**, *83*, 381−403.
(30) Fox, T.; Kollman, P. A. *J. Phys. Chem. B* **1998**, *102*, 8070−8079.
(31) Neumann, M. *Mol. Phys.* **1983**, *50*, 841−858.
(32) Allen, M. P.; Tildesley, D. J. *Computer Simulations of Liquids*; Oxford University Press: New York, 1987.
(33) Cornell, W. D.; Cieplak, P.; Bayly, C. I.; Gould, I. R.; Merz, K. M. Jr.; Ferguson, D. M.; Spellmeyer, D. C.; Fox, T.; Caldwell, J. W.; Kollman, P. A. *J. Am. Chem. Soc.* **1995**, *117*, 5179−5197.
(34) Watts, H.; Alder, B. J.; Hildebrand, J. H. *J. Chem. Phys.* **1955**, *23*, 659−661.
(35) Bender, H. J.; Zeidler, M. D. *Ber. Bunsen-Ges. Phys. Chem.* **1971**, *75*, 236−242.
(36) Harris, K. R.; Lam, H. N.; Raedt, E.; Easteal, A. J.; Price, W. E.; Woolf, L. A. *Mol. Phys.* **1990**, *71*, 1205−1221.
(37) Brier, P. N.; Perry, A. *Adv. Mol. Relax. Interact. Processes* **1978**, *13*, 1−46.
(38) Sprik, M. *J. Chem. Phys.* **1991**, *95*, 6762−6769.
(39) Pusztai, L.; McGreevy, R. L. *Mol. Phys.* **1997**, *90*, 533−539.
(40) van der Spoel, D.; van Maaren, P. J. *J. Chem. Theory Comput.* **2006**, *2*, 1−11.
(41) Höchtl, P.; Boresch, S.; Bitomsky, W.; Steinhauser, O. *J. Chem. Phys.* **1998**, *109*, 4927−4937.
(42) Chatterjee, S.; Debenedetti, P. G.; Stillinger, F. H.; Lynden-Bell, R. M. *J. Chem. Phys.* **2008**, *128*, 124511.
(43) Mills, R. *J. Phys. Chem.* **1973**, *77*, 685−688.
(44) Kusalik, P. G.; Svishchev, I. M. *Science* **1994**, *265*, 1219−1221.
(45) Sorenson, J. M.; Hura, G.; Glaeser, R. M.; Head-Gordon, T. *J. Chem. Phys.* **2000**, *113*, 9149−9161.
(46) Hura, G.; Russo, D.; Glaeser, R. M.; Head-Gordon, T.; Krack, M.; Parrinello, M. *Phys. Chem. Chem. Phys.* **2003**, *5*, 1981−1991.
(47) Hoy, A. R.; Bunker, P. R. *J. Mol. Spectrosc.* **1979**, *74*, 1−8.
(48) Soper, A. K.; Phillips, M. G. *Chem. Phys.* **1986**, *107*, 47−60.
(49) Báez, L. A.; Clancya, P. *J. Chem. Phys.* **1994**, *101*, 9837−9840.
(50) Kell, G. S. *J. Chem. Eng. Data* **1975**, *20*, 97−105.
(51) Wagner, W.; Pruss, A. *J. Phys. Chem. Ref. Data* **2002**, *31*, 387−535.
(52) Billeter, S. R.; King, P. M.; van Gunsteren, W. F. *J. Chem. Phys.* **1994**, *100*, 6692−6699.